Image-domain full waveform inversion

Sanzong Zhang and Gerard Schuster
King Abdullah University of Science and Technology

Summary

The main difficulty with the data-domain full waveform inversion (FWI) is that it tends to get stuck in the local minima associated with the waveform misfit function. This is because the waveform misfit function is highly nonlinear with respect to changes in velocity model. To reduce this nonlinearity, we define the image-domain objective function to minimize the difference of the suboffset-domain common image gathers (CIGs) obtained by migrating the observed data and the calculated data. The derivation shows that the gradient of this new objective function is the combination of the gradient of the conventional FWI and the image-domain differential semblance optimization (DSO). Compared to the conventional FWI, the image-domain FWI is immune to cycle skipping problems by smearing the nonzero suboffset images along wavepath. It also can avoid the edge effects and the gradient artifacts that are inherent in DSO due to the falsely over-penalized focused images. This is achieved by subtracting the focused image associated with the calculated data from the unfocused image associated with the observed data in the image-domain misfit function. The numerical results of the Marmousi model show that image-domain FWI is less sensitive the initial model than the conventional FWI.

Introduction

Prestack depth migration of seismic data is the industry standard for computing detailed estimates of the earth's reflectivity distribution. However, an accurate velocity model is a precondition for imaging complex geological structures. To improve the resolution of the velocity model, the wave-equation tomography is proposed to invert the waveform information for fine details of the earth model (Tarantola, 1986, 1987; Mora, 1987; Woodward, 1992; Luo and Schuster, 1991a and 1991b; Crase et al., 1992; Zhou et al., 1995; Pratt, 1998). These methods can be mainly divided into two categories. The first category defines the objective function in the data domain to best fit the travelitme or waveform information in the observed data. The second category defines an objective function in the image domain to flatten the angle-domain, offset-domain or shot-domain CIGs or focus the sub-offset CIGs.

FWI is a kind of the data-domain wave-equation inversion method. The objective function of FWI is the waveform residual between the observed data and modeled data. This objective function is minimized by smearing the waveform residual along the wavepath calculated from the initial velocity model to update the velocity model. A finely detailed velocity model can be inverted if the initial velocity model is close to the true velocity model. The problem with FWI is that its objective function can be highly nonlinear with respect to velocity perturbations. Therefore, a gradient-based optimization method will get stuck in a local minima and cycle skipping if the initial velocity model is far from the true velocity model. To reduce the nonlinearity, FWI requires the low frequency or long-offset components in the observed data.

Wave-equation migration velocity analysis (WEMVA) is an image-domain wave-equation inversion method that uses numerical solutions to the one-way or two-way wave equation. Several WEMVA methods have been proposed to extract velocity information from the migration image. DSO (Symes and Kern, 1994) uses the first derivative of the migration image along the angle axis to produce the image perturbation. It also uses the suboffset to construct a penalty operator, which annihilates the energy at nonzero lags, and enhance the energy at zero lags. This objective function can avoid the cycle skipping problem, but will falsely over-penalize an already focused CIGs with variant amplitudes (Zhang and Biondo, 2012). It also has difficulties with the unfocused images in complex subsurface regions due to poor illumination even if the velocity is correct (Tang and Sava, 2012). Sava and Biondi (2004) use Stolt residual migration to construct image perturbations. Since Stolt migration only assumes a constant velocity for the entire model to migrate the seismic data, it does not always provide the correct velocity update. Yang and Sava (2011) use the time-lag image condition to construct image perturbations with the assumption that the time-lag must be very small and picked at each iteration. Almomin (2011) presents a new method to measure the image perturbation using the cross-correlation of the observed image with a reference image in the reflection angle gather. The objective function is the depth shift between the observed image and the calculated image. The velocity is updated by smearing this depth residual along the wavepath. Since the observed image is difficult to determine in practice, it is approximated by the calculated image under the small perturbation assumption. The merit of this method is that it is less sensitive to the amplitude of the observed data. Following Almomin's work, Zhang et al (2012) extracted the velocity information by maximizing the angle stack power of angle-domain CIGs. This method relates the image gather flatness objective function to an intermediate moveout parameter. The image perturbation is constructed from this moveout

DOI http://dx.doi.org/10.1190/segam2013-1238.1

parameter based on the fact that the moveout parameter describes the kinematic change in the angle-domain CIGs caused by velocity perturbations.

This paper proposed a new image-domain wave-equation inversion method, which minimizes the difference of the suboffset-domain image obtained by migrating the waveform residual in the data-domain. The gradient of this objective function is composed of two parts. One part smears the zero suboffset image residual along wavepath to update the velocity model. Similar to the conventional FWI, this term has the cycle skipping problem when the initial velocity model is far from the true velocity model. The second part smears the non-zeros suboffset image along wavepath to update the velocity model. This term does not have the cycle skipping problem like DSO. However, the conventional DSO has the edge effect and the unfocused images in complex region with poor illumination even if the velocity model is correct. This will creates a lot of gradient artifacts for velocity updates. Image-domain FWI method can avoid these faults by subtracting the focused suboffset-domain images calculated from the initial velocity model associated the modeled data from the unfocused suboffset-domain image associated with the observed data.

This paper begins with the introduction the theory and method of image-domain FWI. Next the mathematical derivation and numerical examples are presented to demonstrate its effectiveness in velocity inversion. The final section draws the conclusion and shows our acknowledges.

Theory

The cross-correlation function between the forward wavefield $d(\boldsymbol{x}, t|x_s)$ and the backward wavefield $u(\boldsymbol{x}, t|x_s)$ can be used to determine the suboffset-domain image

$$I(\boldsymbol{x}, \boldsymbol{h}) = \int d\,\boldsymbol{x_s} \int d(\boldsymbol{x}-\boldsymbol{h}, t|\boldsymbol{x_s}) u(\boldsymbol{x}+\boldsymbol{h}, t|\boldsymbol{x_s}) dt\,, \quad (1)$$

where the suboffset vector $\boldsymbol{h}$ is the space shift with respect to the trial image location $\boldsymbol{x}$. $d(\boldsymbol{x}, t|\boldsymbol{x_s})$ represents the forward propagation wavefield at $\boldsymbol{x}$ from the source at $\boldsymbol{x_s}$,

$$d(\boldsymbol{x}, t|\boldsymbol{x_s}) = W(t) * G(\boldsymbol{x}, t|\boldsymbol{x_s}), \quad (2)$$

where $W(t)$ is the source wavelet, $G(\boldsymbol{x}, t|\boldsymbol{x_s})$ is the Green function at $\boldsymbol{x}$ with the source initiated at $\boldsymbol{x_s}$, and $*$ is the convolution operator. $u(\boldsymbol{x}, t|\boldsymbol{x_s})$ represents the backward propagation wavefield at $\boldsymbol{x}$ from the receivers at $\boldsymbol{x_g}$,

$$u(\boldsymbol{x}, \boldsymbol{h}) = \int d(\boldsymbol{x_g}, t|\boldsymbol{x_s}) * G(\boldsymbol{x}, -t|\boldsymbol{x_g}) d\,\boldsymbol{x_g}\,. \quad (3)$$

The suboffset images can be an indicator of the accuracy for the migration velocity model. The accurate velocity model should focus the image at zero suboffset ($\boldsymbol{h} = \boldsymbol{0}$). A nonzero value of the space shift of the image indicates an inaccuracy in velocity model.

The inverse problem is defined as finding a velocity model that minimizes the following misfit function,

$$\epsilon = \frac{1}{2} \sum_{\boldsymbol{h}} \sum_{\boldsymbol{x}} [I_{obs}(\boldsymbol{x}, \boldsymbol{h}) - I_{cal}(\boldsymbol{x}, \boldsymbol{h})]^2, \quad (4)$$

where $I_{obs}(\boldsymbol{x}, \boldsymbol{h})$ and $I_{cal}(\boldsymbol{x}, \boldsymbol{h})$ are the suboffset-domain image obtained by migrating the observed data and the modeled data. The optimal estimate of velocity model minimizes the image intensity of the nonzero suboffset gathers and focus the image at the zero suboffset. $I_{obs}(\boldsymbol{x}, \boldsymbol{h})$ spreads the image energy at nonzero lags if there are errors in velocity model. Since the forward modeling and migration use the same velocity model, $I_{cal}(\boldsymbol{x}, \boldsymbol{h})$ is always the focused image. The exception is that $I_{cal}(\boldsymbol{x}, \boldsymbol{h})$ does not only focus at zero suboffset, but spread some image energy along the no-zero suboffsets in the complex region with poor illumination. This phenomenon violates the criterion of DSO. Compared with DSO, image-domain FWI removes these effects by subtracting the background focused image associate with the modeled data from the unfocused image associated with the observed data.

Taking the derivative of ϵ with respect to velocity perturbations yields the misfit gradient

$$\gamma(\boldsymbol{x}') = -\sum_{\boldsymbol{h}} \sum_{\boldsymbol{x}} \Delta I(\boldsymbol{x}, \boldsymbol{h}) \frac{\partial I(\boldsymbol{x}, \boldsymbol{h})}{\partial c(\boldsymbol{x}')}. \quad (5)$$

Here for simplicity, we use $I(\boldsymbol{x}, \boldsymbol{h})$ instead $I_{obs}(\boldsymbol{x}, \boldsymbol{h})$ to represent the suboffset-domain image obtained by migrating the observed data. $\Delta I(\boldsymbol{x}, \boldsymbol{h})$ is the suboffset-domain image residual,

$$\Delta I(\boldsymbol{x}, \boldsymbol{h}) = I_{obs}(\boldsymbol{x}, \boldsymbol{h}) - I_{cal}(\boldsymbol{x}, \boldsymbol{h}). \quad (6)$$

$\frac{\partial I(\boldsymbol{x}, \boldsymbol{h})}{\partial c(\boldsymbol{x}')}$ is called the tomographic operator which actually denotes the reflection wavepath. The physical meaning of equation (5) is that the gradient of image-domain FWI is obtained by smearing suboffset-domain image residual along the wavepath.

Substituting (1) to the tomographic operator, we can get

DOI http://dx.doi.org/10.1190/segam2013-1238.1

$$\frac{\partial I(\boldsymbol{x},\boldsymbol{h})}{\partial c(\boldsymbol{x}')} = \int d\,\boldsymbol{x}_s \int \left[\frac{\partial d(\boldsymbol{x}-\boldsymbol{h},t|\boldsymbol{x}_s)}{\partial c(\boldsymbol{x}')} u(\boldsymbol{x}+\boldsymbol{h},t|\boldsymbol{x}_s) + \frac{\partial u(\boldsymbol{x}+\boldsymbol{h},t|\boldsymbol{x}_s)}{\partial c(\boldsymbol{x}')} d(\boldsymbol{x}-\boldsymbol{h},t|\boldsymbol{x}_s)\right] dt\,. \quad (7)$$

Under Born approximation, we can have the following formula,

$$\frac{\partial d(\boldsymbol{x}-\boldsymbol{h},t|\boldsymbol{x}_s)}{\partial c(\boldsymbol{x}')} = \frac{2}{c^3(x')}\ddot{d}(\boldsymbol{x}',t|\boldsymbol{x}_s) * G(\boldsymbol{x}',t|\boldsymbol{x}-\boldsymbol{h}), \quad (8)$$

and

$$\frac{\partial u(\boldsymbol{x}+\boldsymbol{h},t|\boldsymbol{x}_s)}{\partial c(\boldsymbol{x}')} = \frac{2}{c^3(x')}\left[\int d(\boldsymbol{x}_g,t|\boldsymbol{x}_s) * G(\boldsymbol{x}',-t|\boldsymbol{x}_g) d\boldsymbol{x}_g\right] * G(\boldsymbol{x}+\boldsymbol{h},-t|\boldsymbol{x}'). \quad (9)$$

Substituting equation (7), (8) and (9) to (5), we can rewrite equation (5) as the summation of two terms,

$$\gamma(\boldsymbol{x}') = \gamma_1(\boldsymbol{x}') + \gamma_2(\boldsymbol{x}'), \quad (10)$$

where

$$\gamma_1(\boldsymbol{x}') = -\frac{2}{c^3(x')}\sum_{\boldsymbol{h}}\sum_{\boldsymbol{x}} \Delta I(\boldsymbol{x},\boldsymbol{h}) \int d\,\boldsymbol{x}_s \int \ddot{d}(\boldsymbol{x}',t|\boldsymbol{x}_s)\,[u(\boldsymbol{x}+\boldsymbol{h},t|\boldsymbol{x}_s) * G(\boldsymbol{x}',-t|\boldsymbol{x}-\boldsymbol{h})]dt, \quad (11)$$

and

$$\gamma_2(\boldsymbol{x}') = -\frac{2}{c^3(x')}\sum_{\boldsymbol{h}}\sum_{\boldsymbol{x}} \Delta I(\boldsymbol{x},\boldsymbol{h}) \int d\,\boldsymbol{x}_s \int \left[\ddot{d}(\boldsymbol{x}-\boldsymbol{h},t|\boldsymbol{x}_s) * G(\boldsymbol{x}',t|\boldsymbol{x}+\boldsymbol{h})\right] u(\boldsymbol{x}',t|\boldsymbol{x}_s)dt\,. \quad (12)$$

Equation (11) and (12) are used to update the velocity model by smear the suboffset-domain image residual $\Delta I(\boldsymbol{x},\boldsymbol{h})$ along wavepath. For zero suboffset ($\boldsymbol{h}=\boldsymbol{0}$), the gradient of image-domain FWI is similar to that of data-domain FWI, but does not contain smile artifacts. For nonzero suboffset, the gradient of image-domain FWI is similar to that of DSO that can handle the cycle skipping problem. The superiority of image-domain FWI to DSO is that it removes the edge effect of suboffset-domain CIGs and does not suffer from the falsely over-penalized focused images. This is achieved by subtracting the focused images of the initial velocity model from the unfocused image.

Examples

To test the effectiveness of image-domain FWI, we applied it to a synthetic data set generated from the Marmousi model shown in Figure 1(a). The data were modeled assuming 242 shots with a 70 meters spacing and a Ricker wavelet with the peak frequency of 15 Hz. The reflected wavefields were recorded by 700 receivers with a fixed spread and 20 meters spacing. We compared the results of two inversion methods (conventional FWI and image-domain FWI) starting from the model shown in Figure 1(b), which was obtained by applying a very strong smoothing to the true model. Both of the conventional FWI and image-domain FWI method were used to invert the observed data. The updated models after 40 iteration are shown in Figures 1(c) and 1(d). The migration images for the two updated models are shown in Figures 1(c, d). Since the initial velocity model is far from the true velocity mode and the observed data has a very high frequency, the conventional FWI failed to converge. The suboffset and angle CIGs for the two inversion results are shown in Figures 3. These results show that the result obtained from image-domain FWI is significantly more accurate than the conventional FWI result. The migration images from the two updated velocity models in Figures 2 indicate that image-domain FWI provides more detailed structure than the conventional FWI method. The suboffset and angle CIGs in Figures 2(a, b, c, d) also illustrate image-domain FWI more accurately focuses the image at zero suboffset and flattens the migration image in the reflection angle gather.

Conclusions

We present image-domain FWI that defines the objective function as the suboffset-domain image residual between the observed data and the calculated data. The gradient of image-domain FWI is a combination of the gradients of the conventional reflection FWI and DSO. Compared to the conventional FWI, image-domain FWI is less sensitive to the initial velocity model and did not have the cycle skipping problem. It can also remove the edge effect and the problem of the falsely over-penalized focused images that are inherent in DSO. Numerical examples demonstrate that for Marmousi data, image-domain FWI provides a more accurate resolution than the conventional FWI, but requires significantly more computation and memory.

Acknowledgments

We thank the 2013 sponsors of Center for Subsurface Imaging and Fluid Modeling (CSIM) at KAUST. We also appreciate the support from IBM Deep Research Center and KAUST High Performance Computing. The intensive computation in this works is conducted in Blue Gene P/Q.

DOI http://dx.doi.org/10.1190/segam2013-1238.1

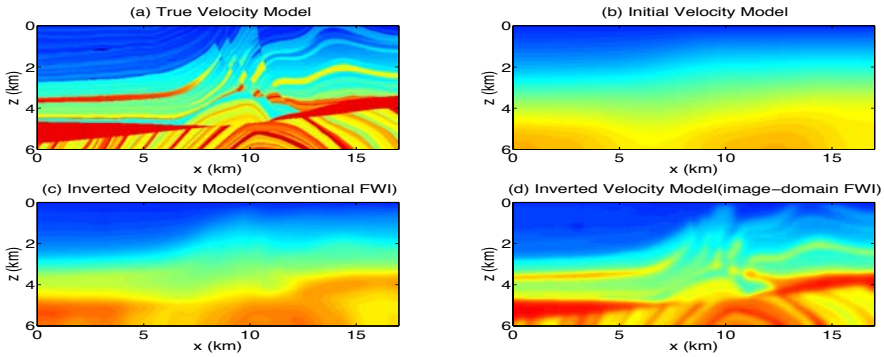

Figure 1: (a) Actual velocity model, (b) initial velocity mode, (c) and (d) inverted velocity model using the conventiona FWI and image-domain FWI.

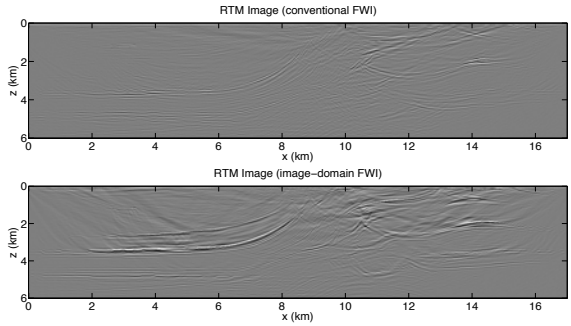

Figure 2: RTM images and CIGs using the inverted velocity model from the conventional FWI and image-domain FWI.

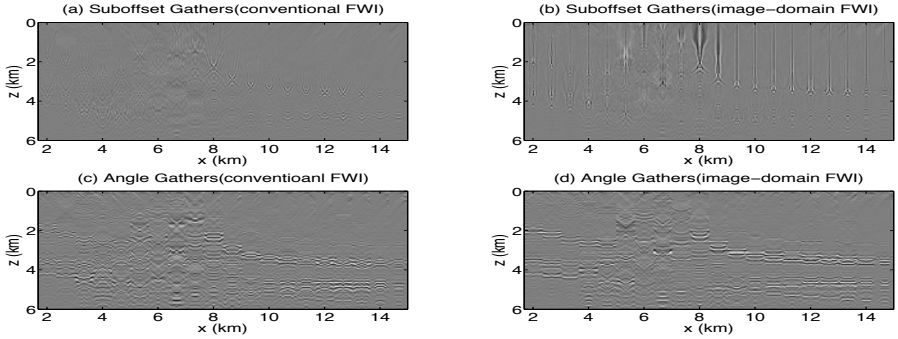

Figure 3: (a) and (b) are the suboffset gathers, and (c) and (d) are the angle gathers using the inverted velocity from the conventional FWI and image-domain FWI.

DOI http://dx.doi.org/10.1190/segam2013-1238.1

http://dx.doi.org/10.1190/segam2013-1238.1

EDITED REFERENCES

Note: This reference list is a copy-edited version of the reference list submitted by the author. Reference lists for the 2013 SEG Technical Program Expanded Abstracts have been copy edited so that references provided with the online metadata for each paper will achieve a high degree of linking to cited sources that appear on the Web.

REFERENCES

Almomin, A., 2011, Correlation based wave equation migration velocity analysis: 81st Annual International Meeting, SEG, Expanded Abstracts, 3887–3891.

Crase, E., C. Wideman, M. Noble, and A. Tarantola, 1992, Nonlinear elastic waveform inversion of landseismic reflection data: Journal of Geophysics Research, **97**, B4, 4685–4704, http://dx.doi.org/10.1029/90JB00832.

Luo, Y., and G. Schuster, 1991a, Wave equation traveltime inversion: Geophysics, **56**, 645–653, http://dx.doi.org/10.1190/1.1443081.

Luo, Y., and G. Schuster, 1991b, Wave equation inversion of skeletonized geophysical data: Geophysical Journal International, **105**, no. 2, 289–294, http://dx.doi.org/10.1111/j.1365-246X.1991.tb06713.x.

Mora, P., 1987, Nonlinear two-dimensional elastic inversion of multioffset seismic data: Geophysics, **52**, 1211–1228, http://dx.doi.org/10.1190/1.1442384.

Sava, P., and B. Biondi, 2004, Wave-equation migration velocity analysis. I. Theory: Geophysical Prospecting, **52**, no. 6, 593–606, http://dx.doi.org/10.1111/j.1365-2478.2004.00447.x.

Pratt, R. G., C. Shin, and G. J. Hicks, 1998, Gauss-Newton and full Newton methods in frequency-space seismic waveform inversion: Geophysical Journal International, **133**, no. 2, 341–362, http://dx.doi.org/10.1046/j.1365-246X.1998.00498.x.

Shen, P., and H. Calandra, 2005, One-way waveform inversion within the framework of adjoint state differential migration: 75th Annual International Meeting, SEG, Expanded Abstracts, 1709–1712.

Symes, W., and M. Kern, 1994, Inversion of reflection seismograms by differential semblance analysis: Algorithm structure and synthetic examples: Geophysical Prospecting, **42**, no. 6, 565–614, http://dx.doi.org/10.1111/j.1365-2478.1994.tb00231.x.

Tarantola, A., 1986, A strategy for nonlinear elastic inversion of seismic reflection data: Geophysics, **51**, 1893–1903, http://dx.doi.org/10.1190/1.1442046.

Tarantola, A., 1987, Inverse problem theory: Elsevier.

Yang, T., and P. Sava, 2011, Wave-equation migration velocity analysis with time-shift imaging: Geophysical Prospecting, **59**, no. 4, 635–650, http://dx.doi.org/10.1111/j.1365-2478.2011.00954.x.

Zhang, Y., and B, Biondi, and Y. Tang, 2012, Residual moveout-based wave-equation migration velocity analysis: 82nd Annual International Meeting, SEG, Expanded Abstracts, http://dx.doi.org/10.1190/segam2012-1123.1.

Zhou, C., W. Cai, Y. Luo, G. Schuster, and S. Hassanzadeh, 1995, Acoustic wave-equation traveltime and waveform inversion of crosshole seismic data: Geophysics, **60**, 765–773, http://dx.doi.org/10.1190/1.1443815.